ICAS 2016
30th Congress of the International Council of the Aeronautical Sciences
DCC, Daejeon, Korea ; September 25-30, 2016

ANALYSIS ON OFFLINE AND ONLINE IDENTIFICATION METHODS FOR AIRCRAFT STABILITY AND CONTROL DERIVATIVES

Ding Di*, Qian Weiqi*, Wang Qing*
*** Computational Aerodynamics Institute of China Aerodynamics Research and Development Center, Sichuan Mianyang, China, 621000**

Abstract

Stability and control characteristics analysis has long been the important research area of aircraft flight dynamics, which is the critical factor of control system design, performance evaluation and integrated design of aircraft. The linear perturbation equations describing aircraft longitudinal and lateral motion, which are derived from nonlinear dynamic equations based on the small perturbation theory, are characterized with matrices called stability and control derivatives in flight control theory. There are two main methods to obtain these derivatives, theoretic deduction and parameter identification, where the latter is a valuable complement for the former one. Offline and online parameter identification are utilized in engineering application with different emphasis. Offline methods are commonly used to obtain linear dynamic model of aircraft under specific operation conditions, with complicated aerodynamic shape or dynamic characteristics, where the model could be used to investigate the stability and control characteristics. Online methods are commonly used in fault detection or flight adaptive control, where the derivatives are estimated with Kalman filters. Aircraft longitudinal and lateral stability and control characteristics are discussed here with online and offline identification methods. Firstly, the small perturbation dynamic equations under rudder perturbation are deduced, and the expressions of all stability and control derivatives are given. Secondly, the Unscented Kalman filter (UKF) method and maximum likelihood estimation (MLE) method are verified with aerodynamic data of a small unmanned aerial vehicle ANCE, where UKF proves to be an adequate online estimation method by the consistent results and its asymptotic approximation to the theoretic values. We also compare the effects of random noises on the estimation accuracy and modes response eigenvalues for these two methods. The results show that UKF has better noise-resistance than MLE, and that UKF prevails in longitudinal derivatives estimation and modes response analysis while maintaining equal performance in lateral direction.

1 Introduction

Stability and control characteristics analysis has long been the important research area of aircraft flight dynamics, which is essential for aircraft control system design, flight quality evaluation and integrated design. Since the invention of the first airplane, people have gradually realized the importance of stability and control analysis which needs to resolve the six degree dynamic equations of aircraft. Then the small perturbation theory analysis method along the aircraft trimmed flight was proposed in the early 20th century because of the limited ability of solving nonlinear equations. The research process of stability and control analysis can be enormously simplified by linearizing the six degree dynamic equations in the case of a small perturbation [1]. The matrix elements of the linearized dynamic equations are called stability and control derivatives, which are usually used to analyze the stability and control characteristics of aircraft. There are many applications of the small perturbation theory in the development process of some new airplanes, such as the unmanned airplane for ecological

conservation ANCE [2], [3]and the cargo transport airplane FAR23 [4]. They used computational fluid dynamics and wind tunnel tests to obtain the airplane's aerodynamic derivatives, and then the stability and control derivatives can be deduced by these. Based on these derivatives the response modes and flight qualities of the airplane can be analyzed and the integrated design can be developed.

Parameter identification becomes more and more important as it shows some advantages in obtaining the stability and control derivatives besides the theory method. There are two kinds of parameter identification methods, i.e. the offline and online identification, are commonly used in aircraft engineering applications with different emphasis. The offline methods can be used to obtain the linear dynamic model of some aircrafts with complicated aerodynamic shape or special dynamic characteristics under specific operation conditions, where the stability and maneuverability can be investigated by the linear model. For example, the linearized dynamic models of a three-lifting-surface aircraft Ecolifger [5], the rotary-wing aircrafts AF25B [6] and VPM M16 [7], are all identified and established by offline methods. The online methods are very useful in flight adaptive control and fault detection, where the aircraft stability and control derivatives are estimated by online identification methods such as Kalman filters. As it is very convenient in computer recursive calculation, Kalman filters become very popular in both online and offline aircraft parameter estimations. For example, F-111 used the Kalman filter to estimate the stability and control derivatives online in its control system design [8]; Kim designed an innovative differential vortex-lattice method tightly coupled with extended Kalman filters [9] and utilized it in the online fault detection of impaired aircraft by giving the approximate location and extent of damages. Meanwhile, the online methods are also utilized in some strong-nonlinear time-varying aerodynamic parameter estimation problems. Vitale utilized UKF algorithm to identify the aerodynamic models in the reentry transonic flow regime of FTB1 (first Flying Test Bed) from the flight data of a dropped transonic flight test mission. In the end he concluded that UKF algorithm has the advantage in good performance of convergence, reduction of uncertainty of the priori aerodynamic model, and capability of extracting the information from a limited flight data [10]; Yu also utilized an augment strong tracking extended Kalman filter [11] (ASTEKF) as the online identification tool to estimate the transonic aerodynamic parameters of a reentry body.

The Maximum Likelihood estimation [12]-[14] (MLE) becomes the widely used method in the area of aircraft dynamic system parameter offline identification as soon as it was proposed by Fisher because of its asymptotic unbiased characteristics. Mehra [15] used the output error and equation error methods with Maximum Likelihood criterion to identify the stability and control derivatives separately from the lateral and longitudinal flight test data of HL-10 and M2/F3, the comparison of identification results show that the MLE method is more accuracy than the equation error method with the absence of both process and measurement noises. Kalman filter is a minimum variance estimation method based on the Gaussian distribution hypothesis, as well as a numerical approximation to the recursive Bayesian estimation problem. In early 1970s, Jazwinski and Gelb expanded the application of Kalman filter in parameter estimation by extending the unknown parameters to the system state variables, which is known as the extended Kalman filter (EKF). In EKF algorithm, the system should be linearized to first order space model by Taylor series expansion. Ignoring the 2nd and higher order terms in the linearization process will lead to bias estimation and increase the possibility of divergence when the system has strongly nonlinear characteristics or inaccurate noise statistical properties. Therefore, the unscented Kalman filter (UKF) is proposed to remedy the flaw of EKF algorithm application in strongly nonlinear systems. The UKF algorithm is based on the deterministic sampling approach, which uses the mean and covariance of a minimal set of deterministically chosen sample points to represent the statistical properties of the state random variables. The UKF algorithm propagated the statistical

properties through the true nonlinear system, so it is equivalent to a second order EKF in accuracy [16]. Brunke and Campbell compared the performance of EKF and the sigma point filter (SPF), and UKF can generally be regarded as one approach of the latter. The conclusion was drawn that EKF diverges quickly but the SPF is more accurate and more amenable than the EKF for real-time estimation applications [17]. Chowdhary and Jategaonkar compared the performance of EKF and UKF algorithms for aerodynamic state/parameter estimation of a fixed wing aircraft (HFB-320) and a rotary wing UAV (ARTIS) from real flight data. The results indicate that the UKF is superior in terms of time to convergence and relative reliability of the estimation than the EKF, however it is computationally more expensive [18]. Li Meng estimated the longitudinal stability and control derivatives and dimensionless coefficients of an oceanographic UAV based the UKF, the results indicate that the UKF algorithm provide excellent performances and the responses match well [19]. Thereby we prefer the UKF in the applications of estimating aircraft stability and control derivatives because of the poor performance of EKF in convergence and stability.

The offline and online parameter estimation methods for the aircraft stability and maneuverability characteristics analysis are discussed in this paper. The aircraft 6DOF dynamic model is linearized by the small perturbation theory, and the expressions of the stability and control derivatives by the aerodynamic derivatives are given. Then we use MLE and UKF as the offline and online estimation methods. A small unmanned aerial vehicle ANCE is taken as a numerical example to validate the two algorithms. Based on the noiseless simulation data, the results indicate that the stability and control derivatives obtained from the two identification methods are similar and close to the analysis values by the small perturbation theory. So we can consider MLE and UKF as effective methods of estimating the aircraft stability and control derivatives. Then further Monte Carlo simulations are carried out to evaluate the performance of UKF and MLE under random noises.

2 Aircraft Linearized Dynamic Models

The 6DOF aircraft dynamic model can be simplified into linear space model by the small perturbation theory, the linear space model can be written as:

$$\begin{aligned} \dot{\mathbf{x}} &= \mathbf{A}\mathbf{x} + \mathbf{B}\mathbf{u} \\ \mathbf{y} &= \mathbf{C}\mathbf{x} + \mathbf{D}\mathbf{u} \end{aligned} \tag{1}$$

Where $\boldsymbol{A}$, $\boldsymbol{B}$ represent the matrices of stability and control derivatives, $\boldsymbol{x}$ is the state vector, $\boldsymbol{u}$ is the input vector, $\boldsymbol{y}$ is the output vector, $\boldsymbol{C}$, $\boldsymbol{D}$ are generally known matrices, and determined by the relationship of the output vector between the state vector and the input vector.

The six degree aircraft dynamic model can be linearized into longitudinal and lateral space models, where the state vector of the longitudinal model can be written as $\boldsymbol{x}=[\Delta V, \Delta\alpha, \Delta q, \Delta\vartheta]^{\mathrm{T}}$, which separately represents the increments of velocity, angle of attack, pitch angular rate and pitch angle, the input of the longitudinal model is the elevator deflection $\Delta\delta_e$, the matrices $\boldsymbol{A}_z$, $\boldsymbol{B}_z$ are expressed in Eq(2); the state vector of the lateral model is noted as $\boldsymbol{x}=[\Delta\beta, \Delta p, \Delta r, \Delta\gamma]^{\mathrm{T}}$, which separately represents the increments of sideslip angle, roll angular rate, pitch angular rate and roll angle, the input vector of the lateral model includes the rudder and the aileron deflections, which is noted as $\boldsymbol{u}=[\Delta\delta_r, \Delta\delta_a]^{\mathrm{T}}$, the matrices $\boldsymbol{A}_h$, $\boldsymbol{B}_h$ are expressed in Eq(3). In the standard term of straight flight, the mathematics relationship of the dimensional stability and control derivatives and the aerodynamic derivatives is expressed in Tab. 1 and Tab. 2.

$$\boldsymbol{A}_z = \begin{bmatrix} X_u & X_\alpha & 0 & X_\vartheta \\ Z_u & Z_\alpha & Z_q & 0 \\ M_u & M_\alpha & M_q & 0 \\ 0 & 0 & 1 & 0 \end{bmatrix} \quad \boldsymbol{B}_z = \begin{bmatrix} X_{\delta e} \\ Z_{\delta e} \\ M_{\delta e} \\ 0 \end{bmatrix} \tag{2}$$

Tab. 1 Dimensional longitudinal stability and control derivatives

$$X_u = -\left(C_{D\bar{u}} + 2C_{D0}\right)u_0^{-1}qS/m$$
$$X_\alpha = \left(C_G - C_{D\alpha}\right)qS/m \quad ..$$
$$Z_u = -\left(C_{L\bar{u}} + 2C_{L0}\right)u_0^{-1}qS/\left(mu_0 + qSC_{L\dot{\alpha}}\right)$$
$$Z_\alpha = -\left(C_{L\alpha} + C_{P0}\right)qS/\left(mu_0 + qSC_{L\dot{\alpha}}\right)$$
$$Z_q = \left(mu_0 - qSC_{Lq}\right)/\left(mu_0 + qSC_{L\dot{\alpha}}\right)$$
$$M_u = \left[\left(C_{M\bar{u}} + 2C_{M0}\right)u_0^{-1} + C_{M\dot{\alpha}}Z_u\right]qSb_A/I_y$$
$$M_\alpha = \left(C_{M\alpha} + C_{M\dot{\alpha}}Z_\alpha\right)qSb_A/I_y$$
$$M_q = \left(C_{Mq} + C_{M\dot{\alpha}}Z_q\right)qSb_A/I_y$$
$$X_{\delta e} = -C_{D\delta e}qS/m$$
$$Z_{\delta e} = -C_{L\delta e}qS/\left(mu_0 + qSC_{L\dot{\alpha}}\right)$$
$$M_{\delta e} = \left(C_{M\delta e} + C_{M\dot{\alpha}}Z_{\delta e}\right)qSb_A/I_y$$

$$\boldsymbol{A}_h = \begin{bmatrix} Y_\beta & Y_p & Y_r & Y_\gamma \\ L_\beta & L_p & L_r & 0 \\ N_\beta & N_p & N_r & 0 \\ 0 & 1 & 0 & 0 \end{bmatrix} \quad \boldsymbol{B}_h = \begin{bmatrix} Y_{\delta r} & Y_{\delta a} \\ L_{\delta r} & L_{\delta a} \\ N_{\delta r} & N_{\delta a} \\ 0 & 0 \end{bmatrix} \tag{3}$$

Tab. 2 Dimensional lateral stability and control derivatives

$Y_\beta = C_{Y\beta}qS/mu_0$	$Y_p = C_{Yp}qS/mu_0$
$Y_r = C_{Yr}qS/mu_0 - 1$	$Y_\gamma = g_0/u_0$
$L_\beta = C_{l\beta}qSl/I_x$	$L_p = C_{lp}qSl/I_x$
$L_r = C_{lr}qSl/I_x$	$N_\beta = C_{n\beta}qSl/I_z$
$N_p = C_{np}qSl/I_z$	$N_r = C_{nr}qSl/I_z$
$Y_{\delta r} = C_{Y\delta r}qS/mu_0$	$Y_{\delta a} = C_{Y\delta a}qS/mu_0$
$L_{\delta r} = C_{l\delta r}qSl/I_x$	$L_{\delta a} = C_{l\delta a}qSl/I_x$
$N_{\delta r} = C_{n\delta r}qSl/I_z$	$N_{\delta a} = C_{n\delta a}qSl/I_z$

3 Identification methods

3.1 Maximum Likelihood method

The Maximum Likelihood estimation combining with the modified Newton-Raphson iteration can be used as the offline parameter estimation method for aircraft stability and control derivatives. The ML criterion is written as [15]:

$$J(\boldsymbol{\theta}) = \sum_{i=1}^{N}[\boldsymbol{v}^T(i)\boldsymbol{R}^{-1}\boldsymbol{v}(i) + \ln|\boldsymbol{R}|] \tag{4}$$

Where $\boldsymbol{v}(i)$ is the output error vector, it can be expressed as:

$$\boldsymbol{v}(i) = \hat{\boldsymbol{y}}(i) - \boldsymbol{y}_m(i)$$

$\hat{\boldsymbol{y}}(i)$ is the simulation output vector from the dynamic model, $\boldsymbol{y}_m(i)$ is the measured output vector, $\boldsymbol{R}$ is the covariance matrix of the observation noise, the unknown parameter vector $\boldsymbol{\theta}$ usually consists of the aircraft stability and control derivatives and the initial state values of the dynamic system.

The modified Newton-Raphson method consists in updating estimation parameters from iteration i to i+1 as:

$$\boldsymbol{\theta}_{i+1} = \boldsymbol{\theta}_i + \Delta\boldsymbol{\theta}_i$$
$$\Delta\boldsymbol{\theta}_i = -\left(\frac{\partial^2 J}{\partial\boldsymbol{\theta}_k\partial\boldsymbol{\theta}_l}\right)^{-1}\left(\frac{\partial J}{\partial\boldsymbol{\theta}_k}\right) \tag{5}$$

Where the Jacobian and Hessian matrices of the ML criterion are expressed as:

$$\begin{cases} \dfrac{\partial J}{\partial\boldsymbol{\theta}_k} = 2\sum_{i=1}^{N}\boldsymbol{v}^{\mathrm{T}}(i)\boldsymbol{R}^{-1}\dfrac{\partial\hat{\boldsymbol{y}}(i)}{\partial\boldsymbol{\theta}_k} \\ \dfrac{\partial^2 J}{\partial\boldsymbol{\theta}_k\partial\boldsymbol{\theta}_l} = 2\sum_{i=1}^{N}\dfrac{\partial\hat{\boldsymbol{y}}^{\mathrm{T}}(i)}{\partial\boldsymbol{\theta}_k}\boldsymbol{R}^{-1}\dfrac{\partial\hat{\boldsymbol{y}}(i)}{\partial\boldsymbol{\theta}_l} \end{cases} \tag{6}$$

The modified Newton-Raphson iteration has superiority over other methods by its quick convergence and high computational efficiency, but the shortcoming is also obvious that the iteration initial values must be strictly chosen and the iteration can be easily divergent.

3.2 Unscented Kalman filter

The Unscented Kalman filter is a recursive minimum mean-square-error (MMSE) estimator based on the optimal Gaussian approximate [16], [18]. Unlike the EKF, the UKF uses the true nonlinear models and a minimal set of deterministically chosen sample points to represent the state distribution. In the UKF, the augmented state random variable is given by the system state vector, the unknown parameter vector, the process and measurement noise vectors:

$$\boldsymbol{x}_k^a = \begin{bmatrix}\boldsymbol{x}_k & \boldsymbol{\theta}_k & \boldsymbol{w}_k & \boldsymbol{v}_k\end{bmatrix}_{L\times 1}^T \tag{7}$$

Where the superscript 'a' denotes the augmented state vector, the process and measurement noises are assumed to be white Gaussian noises with zero means and covariance matrices $\boldsymbol{R}_w$ and $\boldsymbol{R}_v$ respectively. The system is extended to L dimensional space.

Then the relative state covariance matrix is written as:

$$\boldsymbol{P}^a = \begin{bmatrix} \boldsymbol{P}_x & 0 & 0 & 0 \\ 0 & \boldsymbol{P}_\theta & 0 & 0 \\ 0 & 0 & \boldsymbol{R}_w & 0 \\ 0 & 0 & 0 & \boldsymbol{R}_v \end{bmatrix}_{L\times L} \tag{8}$$

The unscented transformation (UT) is a method to constitute a set of sigma points to approximate the statistics of a random variable which undergoes a nonlinear transformation. Based on the UT the scaled unscented transformation (SUT) uses a scaling parameter to control the sigma points without causing the covariance to become non-positive semidefinite. A set of SUT sigma points are noted as $\boldsymbol{S} = \{\varpi_i, \boldsymbol{\chi}_i; i = 0, \cdots, 2L\}$, where ϖ_i is the weight associated with the ith sigma point, superscript 'm' and 'c' denote weights for the computation of mean and covariance respectively, $\boldsymbol{\chi}_i$ is the ith sigma points, it can be expressed as:

$$\begin{cases} \boldsymbol{\chi}_0 = \bar{\boldsymbol{x}} \\ \boldsymbol{\chi}_i = \bar{\boldsymbol{x}} + \left(\sqrt{(L+\lambda)\boldsymbol{P}_x}\right)_i, i = 1, \cdots, L \\ \boldsymbol{\chi}_i = \bar{\boldsymbol{x}} - \left(\sqrt{(L+\lambda)\boldsymbol{P}_x}\right)_i, i = L+1, \cdots, 2L \end{cases}$$

$$\begin{cases} \varpi_0^{(m)} = \dfrac{\lambda}{L+\lambda}, i = 0 \\ \varpi_0^{(c)} = \dfrac{\lambda}{L+\lambda} + \left(1 - \alpha^2 + \beta\right), i = 0 \\ \varpi_i^{(m)} = w_i^{(c)} = \dfrac{1}{2(L+\lambda)}, i = 1, \cdots, 2L \end{cases} \tag{9}$$

Where α, β are constants, κ, λ are scaling parameters, λ is expressed in Eq (10), usually choose $\kappa \geq 0$ to guarantee positive semi-definiteness of the covariance matrix, the value of κ is not critically limited, a good default choice is $\kappa = 0$; Choose $0 \leq \alpha \leq 1$, α controls the size of the sigma point distribution and should choose a small number to make the sampling points spread in small area; β is a non-negative weighting term which can be used to represent the higher order moments of the distribution, the optimum value is $\beta = 2$ for the Gaussian distribution.

$$\lambda = \alpha^2 (L + \kappa) - L \tag{10}$$

The standard UKF algorithm consisting of a prediction and an update step is summarized as follows:

1) Initialization. The initial values of the augmented state vector and its covariance given by prior knowledge are written as:

$$\begin{aligned} \hat{\boldsymbol{x}}_0^a &= E\left[\boldsymbol{x}_0^a\right] = \begin{bmatrix} \hat{\boldsymbol{x}}_0^T & \boldsymbol{\theta}_0^T & 0 & 0 \end{bmatrix}^T \\ \hat{\boldsymbol{P}}_0^a &= E\left[\left(\boldsymbol{x}_0^a - \hat{\boldsymbol{x}}_0^a\right)\left(\boldsymbol{x}_0^a - \hat{\boldsymbol{x}}_0^a\right)^T\right] \end{aligned} \tag{11}$$

2) Calculate $2L+1$ sigma points by the SUT:

$$\hat{\boldsymbol{\chi}}_k^a = \begin{bmatrix} \hat{\boldsymbol{x}}_k^a & \hat{\boldsymbol{x}}_k^a - \gamma\sqrt{\hat{\boldsymbol{P}}_k^a} & \hat{\boldsymbol{x}}_k^a + \gamma\sqrt{\hat{\boldsymbol{P}}_k^a} \end{bmatrix} \tag{12}$$

Where parameter γ is expressed as:

$$\gamma = \sqrt{L + \lambda}$$

3) Predict the (k+1)th state vector and its covariance by the kth step:

$$\begin{aligned} \tilde{\boldsymbol{\chi}}_{k+1}^a &= f_d\left(\hat{\boldsymbol{\chi}}_k^x, \boldsymbol{u}_k, \hat{\boldsymbol{\chi}}_k^w\right) \\ \tilde{\boldsymbol{x}}_{k+1}^a &= \sum_{i=0}^{2L} \varpi_i^{(m)} \hat{\boldsymbol{\chi}}_{i,k+1}^a \\ \tilde{\boldsymbol{P}}_{k+1} &= \sum_{i=0}^{2L} \varpi_i^{(c)} \left[\tilde{\boldsymbol{\chi}}_{i,k+1}^x - \tilde{\boldsymbol{x}}_{k+1}\right]\left[\tilde{\boldsymbol{\chi}}_{i,k+1}^x - \tilde{\boldsymbol{x}}_{k+1}\right]^T \end{aligned} \tag{14}$$

Where $f_d(\cdot)$ is the system state function with the process noise, $\boldsymbol{\chi}^x$ corresponds to the state vector and the unknown parameters, $\boldsymbol{\chi}^w$ and $\boldsymbol{\chi}^v$ correspond to the process and measurement noise respectively.

4) Update the prediction by the measurement values. The output vector and its covariance can be calculated by the predicted state vector:

$$\begin{aligned} \boldsymbol{Y}_{k+1} &= g_d\left(\tilde{\boldsymbol{\chi}}_{k+1}^x, \boldsymbol{u}_{k+1}, \tilde{\boldsymbol{\chi}}_{k+1}^v\right) \\ \tilde{\boldsymbol{y}}_{k+1} &= \sum_{i=0}^{2L} \varpi_i^{(m)} \boldsymbol{Y}_{i,k+1} \\ \boldsymbol{P}_{\tilde{y}\tilde{y}_{k+1}} &= \sum_{i=0}^{2L} \varpi_i^{(c)} \left[\boldsymbol{Y}_{i,k+1} - \tilde{\boldsymbol{y}}_{k+1}\right]\left[\boldsymbol{Y}_{i,k+1} - \tilde{\boldsymbol{y}}_{k+1}\right]^T \\ \boldsymbol{P}_{\tilde{x}\tilde{y}_{k+1}} &= \sum_{i=0}^{2L} \varpi_i^{(c)} \left[\tilde{\boldsymbol{\chi}}_{i,k+1}^x - \tilde{\boldsymbol{x}}_{k+1}\right]\left[\boldsymbol{Y}_{i,k+1} - \tilde{\boldsymbol{y}}_{k+1}\right]^T \end{aligned} \tag{15}$$

Where $g_d(\cdot)$ is the extended observation function with measurement noise. The gain matrix is calculated by the covariance matrices in Eq(16).

$$\boldsymbol{K}_{k+1} = \boldsymbol{P}_{\tilde{x}\tilde{y}_{k+1}} \boldsymbol{P}_{\tilde{y}\tilde{y}_{k+1}}^{-1} \tag{16}$$

The system state vector and covariance are updated by the gain matrix in Eq(17).

$$\begin{aligned} \hat{\boldsymbol{x}}_{k+1} &= \tilde{\boldsymbol{x}}_{k+1} + \boldsymbol{K}_{k+1}\left(\boldsymbol{z}_{k+1} - \tilde{\boldsymbol{y}}_{k+1}\right) \\ \hat{\boldsymbol{P}}_{k+1} &= \tilde{\boldsymbol{P}}_{k+1} - \boldsymbol{K}_{k+1} \boldsymbol{P}_{\tilde{y}\tilde{y}_{k+1}} \boldsymbol{K}_{k+1}^T \end{aligned} \tag{17}$$

If the noises are accumulated white noise, then the augmented state vector (in Eq(7)) can get rid of the process and measurement noise,

hence the augmented state vector is given by $\boldsymbol{x}_k^a = \left[\boldsymbol{x}_k^T \quad \boldsymbol{\theta}_k^T\right]^T$, the covariance matrices of process and measurement noise $\boldsymbol{R}_w$ and $\boldsymbol{R}_v$ can be simply added to the right sides of $\tilde{P}_{k+1}$ and $P_{\tilde{y}\tilde{y}_{k+1}}$, which are expressed in Eq(18) and Eq(19). Then the reduced size of system dimension can increase the computational efficiency.

$$\tilde{\boldsymbol{P}}_{k+1} = \sum_{i=0}^{2L} \varpi_i^{(c)} \left[\tilde{\boldsymbol{\chi}}_{i,k+1}^x - \tilde{\boldsymbol{x}}_{k+1}\right]\left[\tilde{\boldsymbol{\chi}}_{i,k+1}^x - \tilde{\boldsymbol{x}}_{k+1}\right]^T + \boldsymbol{R}_w \quad (18)$$

$$\boldsymbol{P}_{\tilde{y}\tilde{y}_{k+1}} = \sum_{i=0}^{2L} \varpi_i^{(c)} \left[\boldsymbol{Y}_{i,k+1} - \tilde{\boldsymbol{y}}_{k+1}\right]\left[\boldsymbol{Y}_{i,k+1} - \tilde{\boldsymbol{y}}_{k+1}\right]^T + \boldsymbol{R}_v \quad (19)$$

Comparing with the EKF algorithm, the UKF algorithm has second order accuracy, and also does not require the function differentiable, that means the Jacobian matrix does not need in the algorithm.

4 Application to Unmanned Aerial Vehicle

4.1 Unmanned Aerial Vehicle

The Unmanned Airplane for Ecological Conservation (ANCE) [2], [3] is used as an example to validate the two identification method. ANCE is a statically stable twin-boom airplane with a maximum take-off mass of 182.055kg, and a rectangular wing of 5.187m of span, and 3.133m^2 of surface area, for an aspect ratio of 8.57. The airplane has a cruise speed of 47.659m/s at 2438m above sea level for a wing Reynolds number of 1.413×10^6. The rolling, pitching and yawing moments of inertia of the airplane are 150, 400, 400kg×m^2 respectively. The longitudinal and lateral aerodynamic derivatives of the airplane are calculated by Computational Fluid Dynamics method in Ref [3]. We can use this UAV as an example to validate the above two identification algorithms.

4.2 Identification methods validation

Simulation data from aircraft six DOF model without noises are used to validate MLE and UFK methods. The small disturbances are separately applied to motivate the longitudinal and lateral dynamic characteristics of UAV in its straight flight state, and then the derivatives are estimated from the simulation data by two identification methods. The results are verified with the theoretic values which are calculated from Tab. 1 and Tab. 2. Tab. 3 and Tab. 4 gives the comparison for MLE and UKF respectively, where MLE and UKF show good consistency with the theoretic values. For all the longitudinal derivatives except the zero-theoretic control derivative $X_{\delta e}$, relative errors are small; while the worst cases of MLE and UKF respectively is X_u and M_u, the absolute values of relative error are 0.76% and 0.45%, this is probably due to the strongly nonlinearity of the velocity dependent terms in the dynamic models. For lateral derivatives, the theoretic value of Y_p is very close to zero, so the relative errors are ignored here as they are too much higher than others for both methods; while the worst cases of MLE and UKF is $Y_{\delta a}$, as its absolute value of relative error is all 7.14% for both MLE and UKF, this is probably due to the dimension of theoretic value is 10^{-3}, which indicates the effects of aileron deflection on the lateral force is small, so the accuracy is relatively poor. From the estimation results, we can find that UKF shows better or equivalent performance than MLE. And nearly 41% of longitudinal derivatives are estimated with accuracy to 10^{-2}, and nearly 43% of lateral derivatives are estimated with accuracy to 10^{-3}, where the reason could be that the nonlinearity of the longitudinal motion is stronger than of the lateral motion.

Fig. 1 and Fig. 2 show the time history of estimation in longitudinal and lateral motion by UKF respectively. The initial values of 12 longitudinal derivatives and 16 lateral derivatives in estimation are set to zero. The UKF estimation results of all derivatives can constringe to theoretic values within 1 second, which shows the capability of application of UKF in the UAV stability and control derivatives online estimation.

Tab. 3 Comparison of UAV longitudinal derivatives results

Longitudinal derivatives	Theory	MLE		UKF	
		Identification	Relative error	Identification	Relative error
X_u	-0.0263	-0.0265	-0.76%	-0.0264	-0.38%
X_α	5.871	5.8866	0.27%	5.8737	0.046%

X_ϑ	-9.81	-9.8191	-0.09%	-9.8098	0.002%
Z_u	-0.0066	-0.0066	0	-0.0066	0
Z_α	-2.6023	-2.5989	0.13%	-2.6010	0.05%
Z_q	0.9811	0.981	-0.01%	0.9811	0
M_u	-0.0221	-0.0221	0	-0.0220	0.45%
M_α	-22.84	-22.8031	0.16%	-22.8103	0.13%
M_q	-1.2105	-1.2105	0	-1.2109	-0.03%
$X_{\delta e}$	0.0	-6.64e-4	-	-1.0381e-4	-
$Z_{\delta e}$	-0.301	-0.3012	-0.07%	-0.3011	-0.03%
$M_{\delta e}$	-16.710	-16.7058	0.03%	-16.7071	0.02%

Tab. 4 Comparison of UAV lateral derivatives results

Lateral derivatives	Theory	MLE		UKF	
		Identification	Relative error	Identification	Relative error
Y_β	-0.1562	-0.1563	-0.06%	-0.1563	-0.06%
Y_p	-1.3e-4	-1.961e-4	-	-1.4921e-4	-
Y_r	-0.9891	-0.989	0.01%	-0.9891	0
Y_γ	0.2058	0.2061	0.15%	0.2058	0
L_β	-19.7095	-19.7086	0.005%	-19.7082	0.007%
L_p	-8.791	-8.7907	0.003%	-8.7906	0.005%
L_r	1.6459	1.6459	0	1.6459	0
N_β	10.1593	10.1598	0.005%	10.1591	-0.002%
N_p	-0.0936	-0.0931	0.53%	-0.0937	-0.11%
N_r	-1.5386	-1.5385	0.007%	-1.5386	0
$Y_{\delta r}$	-0.1342	-0.1346	-0.3%	-0.1342	0
$Y_{\delta a}$	-0.0014	-0.0013	7.14%	-0.0015	-7.14%
$L_{\delta r}$	-2.4368	-2.437	-0.008%	-2.4369	-0.0041%
$L_{\delta a}$	-61.6369	-61.6354	0.002%	-61.6345	0.004%
$N_{\delta r}$	15.6959	15.6955	-0.003%	15.6958	-0.001%
$N_{\delta a}$	0.9138	0.9143	0.05%	0.9138	0

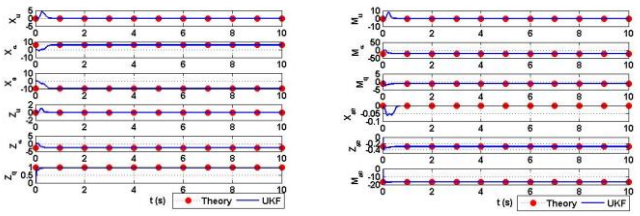

Fig. 1 Time history of UAV longitudinal derivatives by UKF

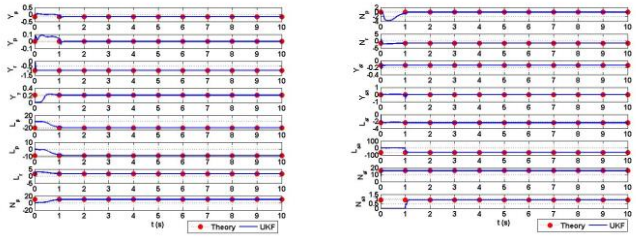

Fig. 2 Time history of UAV lateral derivatives by UKF

4.3 Analysis of random measurement noises

We directly apply additive white noises on the longitudinal and lateral noiseless simulation data, where standard deviations of the noises are proportional to the maximum ranges of corresponding state variables. For velocities the ratio is 2%, angles 1%, and angular velocities 0.1%. 5000 sets of white noises are generated to analyze the effect on stability and control derivative estimation accuracy.

Tab. 5 shows the confidence statistics of longitudinal and lateral derivative estimation results. When relative errors in $\pm$ 10% are regarded as close enough to the theoretic values, and then confidence statistics probabilities are the ratios of the estimations that achieve $\pm$10% relative error to the total number of tests. The confidence statistics in Tab 5 means to reveal different effect on estimating accuracy of random noises. The longitudinal results show that UKF for X_ϑ, Z_α, Z_q, M_α, M_q, and $M_{\delta e}$, the confidence probabilities are 100%, and for X_α and $Z_{\delta e}$ are 95%; while for MLE, only the confidence probabilities of estimation of Z_q and $M_{\delta e}$ are higher than 90%. These results show that UKF is proved to be reliable and prevails over MLE in longitudinal derivatives estimation, which reveal filtering mechanism in UKF provides capability of noise-resistance. For derivatives related to velocities, X_u, Z_u and M_u, where $X_{\delta e}$ is not included due to its zero nominal value, the confidence probabilities are relatively low. These can be traced to the higher level of noise standard deviation relative to velocities in the simulation set-up. For lateral derivatives, because the weaker noise applied, the differences of two methods in estimation confidence probabilities are not significant.

Both MLE and UKF show good performance in all 5 derivatives related to rolling motion, 3 derivatives related to yaw motion (N_β, N_r, and $N_{\delta r}$), and derivative related to lateral motion (Y_r); while for derivatives with very small nominal values (Y_p, N_p, and $Y_{\delta a}$), both the two methods show weak performance.

Tab. 5 Confidence of UAV longitudinal and lateral derivatives estimation

Longitudinal derivatives	Confidence		Lateral derivatives	Confidence	
	MLE %	UKF %		MLE %	UKF %
X_u	10.3	31.04	Y_β	52.76	10.86
X_α	46.14	99.84	Y_p	0.16	0
X_ϑ	67.9	100	Y_r	100	100
Z_u	13.12	14.46	Y_γ	30.5	19.56
Z_α	89.24	100	L_β	100	100
Z_q	92.52	100	L_p	100	100
M_u	6.2	8.12	L_r	100	100
M_α	57.4	100	N_β	100	100
M_q	52	100	N_p	35.54	0
$X_{\delta e}$	0.02	0.04	N_r	100	100
$Z_{\delta e}$	31.46	97.84	$Y_{\delta r}$	32.58	38.6
$M_{\delta e}$	98.4	100	$Y_{\delta a}$	0.18	0
			$L_{\delta r}$	99.9	98.04
			$L_{\delta a}$	100	100
			$N_{\delta r}$	100	100
			$N_{\delta a}$	86.38	14.4

The errors in estimated longitudinal and lateral derivatives due to the random noises will cause dispersion in the response eigenvalues. Fig. 3 and Fig. 4 show the distribution of longitudinal and lateral eigenvalues with and without noises for five response modes, where horizontal axes denote the real part of the eigenvalues, vertical axes denote imaginary part, and where markers '■' and '.' represent MLE results for noise-free cases and noise cases respectively, and '●' and '+' represent UKF results. Fig. 3 reveals that for phugoid mode and short period mode, MLE results suffered stronger dispersion than UKF results, and that MLE result for phugoid mode, the stability of the motion are affected, where a pair of imaginary roots with negative real part becomes real roots or even positive real roots. For UKF results, the eigenvalues maintain a pair of imaginary roots, only in 2.3% out of 5000 simulations appears false positive real part of the eigenvalues, in which the dynamics of the system will exhibit oscillation & divergent characteristics. For short period mode, both methods show good consistency in eigenvalues with negative real part, which guarantees the stability or asymptotic stability of the system. The minor portion of MLE estimation results, i.e. 5%, appears eigenvalues with zero imaginary part, which will cause the corresponding motion mode to vanish in periodicity. Fig. 4 shows that, for three lateral modes, noises applied here have limited effect on the dispersion and characteristics of eigenvalues by both methods, which mean the lateral response modes analysis is reliable based on the parameter estimation methods.

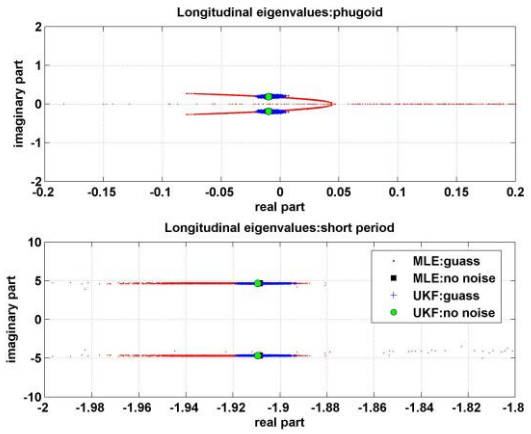

Fig. 3 Noise effect on UAV longitudinal modes response eigenvalues

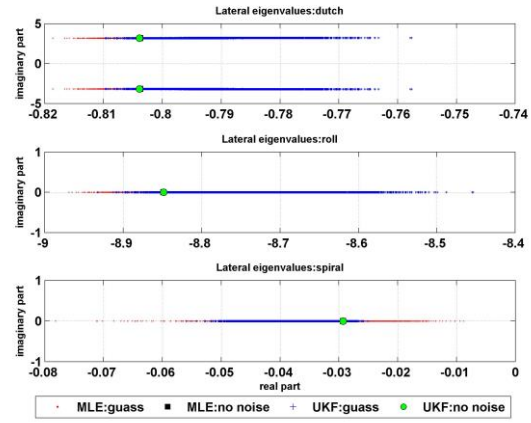

Fig. 4 Noise effect on UAV lateral modes response eigenvalues

Based on the Monte Carlo simulation results, the confidence statistics probabilities of the two methods for UAV longitudinal and lateral response mode eigenvalues estimation under random noises are shown in Tab. 6. Firstly, the criterion of reliable mode eigenvalues is to maintain response characteristics of the system, which mean the asymptotically convergent and periodical motion does not degenerate to non-convergent or non-periodical motion. And the second criterion is to demand the mold of

eigenvalues within $\pm 10\%$ of their noise-free counterparts. Based on the statistics presented in Tab. 6, under the current random noises characteristics, UKF prevails MLE for most of the cases as phugoid mode and short-period mode, while for spiral mode, MLE results are slightly better than UKF results. For Dutch mode and roll mode, both methods achieve 100% confidence, which prove the validity of the estimation methods on analyzing the two response modes. For phugoid mode and spiral mode, the estimation processes are heavily affected by noises applied, which produces low probability of reliable results. The reason could be the relatively small real parts for these two modes eigenvalues, where noises could cover the true characteristics of the UAV and make it difficult to estimate eigenvalues of the motion mode from contaminated data.

Tab. 6 Confidence of UAV modes response analysis

Modes response		MLE %	UKF %
Longitudinal	Phugoid	22.58	76.66
	Short-period	94.64	100
Lateral	Dutch	100	100
	Roll	100	100
	Spiral	30.56	20.5

5 Conclusions

In this paper, we tried to fulfill the stability and control characteristics analysis requirement in UAV development, and discussed the application of parameter estimation methods in aircraft stability and control derivatives estimation. We used MLE and UKF as offline and online estimation algorithms respectively, and applied them to an UAV example. Based on simulation data collected under three directional rudder deflections, we compared the online and offline results obtained by estimation with the theoretic results based on small perturbation theory, which proves the validity of the methods. Then we carried out Monte Carlo (5000 times) simulation with noises in longitudinal and lateral motion. By comparing the effect of noises on the estimation accuracy of two methods and on the UAV response mode eigenvalues, we achieved some conclusions:

1) Longitudinal and lateral derivatives estimation with MLE and UKF show good consistency. Lateral derivatives agree with the theoretic results with higher accuracy due to the linearity of lateral motion. UKF exhibits responsive convergence performance, and proves to be an efficient online estimation method for UAV aerodynamic derivatives.
2) From noisy data, UKF implements a dynamic process of filtering, while MLE is known as vulnerable to noises. The results show that UKF has better performance for high-noise cases and is equivalent to MLE in low-noise cases.
3) For derivatives asymptotically approximate to zero, neither UKF nor MLE has good estimation accuracy.
4) For mode response eigenvalues under noises, estimation results also show different confidence levels. The mode results of short-period, Dutch-roll and roll modes can be estimated with higher level of confidence; while confidence levels of phugoid and spiral modes results are relatively lower. Furthermore, noise data can affect the characteristics of estimation results, e.g., from periodical to non-periodical, or from stable to unstable.

The research work in this paper is just a preliminary work about the MLE and UKF for estimating the stability and control derivatives of aircraft. The influence of the environment and measurement noises in actual flight data on the accuracy, stability and convergence of the algorithms is evaluated for MLE and UKF with Monte Carlo simulations. In next step, possible improvement of the MLE and the UKF algorithms needs to be investigated with more insight combining the flight data.

References

[1] Roskam J. Evolution of airplane stability and control: a designer's viewpoint. *J. GUIDANCE*, Vol. 14, No. 3, pp 481-491, 1991.

[2] Cardenas E, Boschetti P and Amerio A. Design of an unmanned aerial vehicle for ecological conservation. *Infotech @ Aerospace*, Arlington Virginia, AIAA 2005-7056, 2005.

[3] Boschetti P, Cardenas E and Amerio A. Stability of an unmanned airplane using a low-order panel method. *AIAA Atmospheric Flight Mechanics Conference*, Ontario Canada, AIAA 2010-8121, 2010.

[4] Biber K. Stability and control characteristics of a new FAR23 airplane. *44th AIAA Aerospace Sciences Meeting and Exhibit*, Reno Nevada, AIAA 2006-255, 2006.

[5] Tang S. Three-lifting-surface aircraft disturbance motion linearized model. *Flight Dynamics*, Vol. 23, No. 1, pp 27-30, 2005.

[6] Yang F, Xiong X and Chen Z. Modeling system identification and validation of small rotorcraft-based unmanned aerial vehicle. *Journal of Beijing University of Aeronautics and Astronautics*, Vol. 36, No. 8, pp 913-917, 2010.

[7] Houston S. Identification of autogyro longitudinal stability and control characteristics. *Journal of Guidance, Control, and Dynamics*, Vol. 21, No. 3, pp 391-399, 1998.

[8] Speyer J, Crues E. On-Line aircraft state and stability derivative estimation using the modified-gain Extended Kalman Filter. *J. GUIDANCE*, Vol. 10, No. 3, pp 262-268, 1987.

[9] Kim J, Palaniappan K and Menon P. Rapid estimation of impaired-aircraft aerodynamic parameters. *Journal of Aircraft*, Vol. 47, No. 4, pp 1216-1228, 2010.

[10] Vitale A, Corraro F and Bernard M. Unscented Kalman filtering for reentry vehicle identification in the transonic regime. *Journal of Aircraft*, Vol. 46, No. 5, pp 1649-1659, 2009.

[11] Yu S, Cheng Y and Qian W. Research on transonic aerodynamic parameter online identification. *Journal of Astronautics*, Vol. 32, No. 6, pp 1211-1216, 2011.

[12] Rauch H, Tung F and Striebel C. Maximum Likelihood estimates of linear dynamic systems. *AIAA Journal*, Vol. 3, No. 8, pp 1445-1450, 1965.

[13] Oshman Y, Mendelboim T. Maximum Likelihood identification and realization of stochastic systems. *Journal of Guidance, Control, and Dynamics*, Vol. 17, No. 4, pp 692-700, 1994.

[14] West N, Swiler L. Parameter estimation via Gaussian Processes and Maximum Likelihood estimation.: *Structures, Structural Dynamics, and Materials Conference 18th*, Orlando Florida, AIAA 2010-2851, 2010.

[15] Mehra R, Stepner D and Tyler J. Maximum Likelihood identification of aircraft stability and control derivatives. *J. AIRCRAFT*, Vol. 11, No. 2, pp 81-89, 1974.

[16] Merwe R. *Sigma-point Kalman filters for probabilistic inference in dynamic state-space models*. Portland: Oregon Health & Science University, 2004.

[17] Brunke S, Campbell M. Square root sigma point filtering for real-time, nonlinear estimation. *J. GUIDANCE*, Vol. 27, No. 2, pp 314-317, 2004.

[18] Chowdhary G, Jategaonkar R. Aerodynamic parameter estimation from flight data applying extended and unscented Kalman Filter. *AIAA Atmospheric Flight Mechanics Conference and Exhibit*, Keystone Colorado, AIAA 2006-6146, 2006.

[19] Li M, Liu L and Veres S. Comparison of linear and nonlinear aerodynamic parameter estimation approaches for an unmanned aerial vehicle using Unscented Kalman Filter. *Journal of Beijing Institute of Technology*, Vol. 20, No. 3, pp 339-344, 2011.

Copyright Statement

Contacts: dingdi1981@cardc.cn.